Temperature-Dependent Energy Gap of the Primary Charge Separation in Photosystem I: Study of Delayed Fluorescence at 77−268 K

ARTICLE *in* THE JOURNAL OF PHYSICAL CHEMISTRY B · JUNE 2008

Impact Factor: 3.3 · DOI: 10.1021/jp710551e · Source: PubMed

5 AUTHORS, INCLUDING:

Shigeru Itoh
Nagoya University
222 PUBLICATIONS **4,110** CITATIONS

SEE PROFILE

Temperature-Dependent Energy Gap of the Primary Charge Separation in Photosystem I: Study of Delayed Fluorescence at 77−268 K

Yutaka Shibata,*,† Shinpei Akai,† Takashi Kasahara,† Isamu Ikegami,‡ and Shigeru Itoh†

Division of Material Science (Physics), Graduate School of Science, Nagoya University, Nagoya 464-8602, Japan and Faculty of Pharmaceutical Sciences, Teikyo University, Sagamiko, Kanagawa 229-0195, Japan

Received: November 2, 2007; Revised Manuscript Received: February 13, 2008

The dynamics of fluorescence decay and charge recombination were studied in the ether-extracted photosystem I reaction center isolated from spinach with picosecond resolution over a wide time range up to 100 ns. At all temperatures from 268 to 77 K, a slow fluorescence decay component with a 30–40 ns lifetime was detected. This component was interpreted as a delayed fluorescence emitted from the singlet excited state of the primary donor P700*, which is repopulated through charge recombination that was increased by the lack of secondary acceptor phylloquinone in the sample. Analysis of the fluorescence kinetics allowed estimation of the standard free-energy difference $-\Delta G$ between P700* and the primary radical pair ($P700^+A_0^-$) state over a wide temperature range. The values of $-\Delta G$ were estimated to be 160/36 meV at 268/77 K, indicating its high sensitivity to temperature. A temperature-dependent $-\Delta G$ value was also estimated in the delayed fluorescence of the isolated photosystem I in which the secondary acceptor quinone was partially prereduced by preillumination in the presence of dithionite. The results revealed that the temperature-dependent $-\Delta G$ is a universal phenomenon common with the purple bacterial reaction centers, photosystem II and photosystem I reaction centers.

I. Introduction

The electron-transfer (ET) steps from the excited primary electron donor to the multiple electron carriers in photosynthetic reaction center (RC) complexes occurs sequentially over a wide time range from femtosecond to seconds. Study of these steps has revealed the essential mechanism of biological electron transfer.[1–8] ET rates are considered to be regulated by two factors: (1) mutual arrangements of the electron carriers and (2) an energy gap determined by the chemical properties of cofactors and their arrangements inside the protein environments.[9,10] X-ray crystallography studies have clearly indicated the structures of multiple RCs.[11,12]

The thermodynamic properties of the electron carriers in RCs have been estimated by various techniques. Photoacoustic measurements[13–16] provided the heat released by the light-induced charge separation reactions and, hence, the standard enthalpy difference ΔH_{CS} and the standard volume change ΔV_{CS}. The values of the standard free-energy difference of the charge-separation reactions ($-\Delta G_{CS}$) in RCs have also been estimated through analysis of the charge-recombination kinetics by measuring the delayed fluorescence (DF)[17–23] or the transient absorption changes.[24–26]

Significant contributions of the entropy change to the total free-energy change have been assumed in the charge-separation reactions in the bacterial RC[14,26] and photosystem (PS) II RC.[19,20] A large contribution of the standard entropy difference, ΔS_{CS}, has also been suggested in the ET reaction to the Fe−S center F_X, F_A, and F_B in the PSI RC.[15,16] The large ΔH_{CS} and ΔS_{CS} values in the above investigations were estimated by assuming these values to be temperature independent. In a classical expression of Marcus' ET theory, ΔS_{CS} of the electron-transfer reaction is assumed to be zero.[27] The apparent temperature-dependent ΔG_{CS} values measured in the charge-separation reactions,[14–20] thus, may come from either the temperature-dependent changes of ΔH_{CS} values or a non-negligible ΔS_{CS} value.

Kleinherenbrink et al.[21] analyzed the temperature dependence of the delayed fluorescence (DF) from PSI at 2–25 °C in a PSII-depleted *Synechocystis* mutant after reducing the secondary electron-acceptor phylloquinone A_1 and estimated the $-\Delta G_{CS}$ and $-\Delta H_{CS}$ values to be 250 and 130 meV, respectively. In this study we measured the DF in the ether-extracted PSI particles in which 90% of antenna chlorophyll *a* (Chl-*a*) molecules and two molecules of the secondary electron acceptor phylloquinone (A_1) were depleted. The special pair P700, the primary electron acceptor Chl-*a* 690 (A_0), and the terminal acceptor iron−sulfur centers F_X, F_A, and F_B remained fully active.[4,28–32] ET from A_0 to F_X was inhibited due to the lack of A_1 in the ether-extracted PSI, and the charge recombination between A_0^- and $P700^+$ was assumed to repopulate the excited state (P700*) and produce DF within a 10–100 ns time range at room temperature as well as at 77 K.[33,34] We also measured the DF in the PSI particles that contain about 200 antenna chlorophyll molecules in the presence of dithionite in which the secondary acceptor A_1 is reduced. We analyzed the dependencies of the DF intensity on temperature and time to estimate the standard free-energy difference of the PSI primary charge-separation reaction. We detected a strong DF even at 77 K, suggesting the lower $-\Delta G_{CS}$ value at the lower temperature, as reported for the PSII and purple bacterial RCs. Similar analysis in the PSI particles also supported this conclusion.

II. Experimental Methods

PSI particles were isolated from spinach by treatment with digitonin as described previously.[28] The freeze-dried PSI

* To whom correspondence should be addressed. Fax: 81-52-789-2883. E-mail: yshibata@bio.phys.nagoya-u.ac.jp.
† Nagoya University.
‡ Teikyo University.

10.1021/jp710551e CCC: $40.75
Published on Web 05/08/2008

particles were extracted with 80% water-saturated diethyl ether as described previously.[28] The number of remaining antenna Chl-*a* molecules per P700 was determined to be 16 based on the absorbance of the antenna Chl-*a* at 677 nm and the absorption change of P700 at 696 nm in the oxidized minus reduced difference spectrum. The PSI particles containing 16 Chls per P700 (designated PSI-16 hereafter) were dissolved in a 50 mM pH 8.5 Tris-HCl buffer containing 0.05% triton X-100 and 10 mM sodium ascorbate. We also used the unextracted PSI particles with about 200 Chl molecules (PSI-200). In the measurement of fluorescence, 50 mM sodium dithionite was added to the sample to reduce the secondary electron acceptor phylloquinones (A_1)[21] to a 200 mM glycine−NaOH buffer (pH 10.5) containing 10 mM sodium ascorbate and 0.02% triton X-100 (designated dtPSI-200 hereafter). A_1^- was accumulated by irradiation of a continuous blue light in the presence of sodium dithionite. The blue excitation light from a 100 W halogen−tungsten lamp through a blue glass filter (C3C 22; Russian Filter, Russia) was focused onto the sample, and the extent of photoaccumulation of A_1^- was estimated by measuring the fluorescence increase during irradiation, according to Kleinherenbrink et al.[21] See Supporting Information for details.

The PS I samples were mixed with glycerol to give a final concentration of 60% (v/v), sealed in an acrylic cell with an optical path length of 1 mm, and then set in a liquid-nitrogen cryostat (DN1704; Oxford Instruments, Inc., Eynsham, U.K.). The temperature of the sample was maintained at 77–268 ± 0.1 K using a temperature controller (ITC4; Oxford Instruments, Inc., Eynsham, U.K.).

The time-resolved fluorescence spectra were measured with a streak-scope system (C4334; Hamamatsu Photonics, Inc., Hamamatsu, Japan) in combination with an excitation diode laser at 405 nm with a pulse duration of 50 ps at a 1 MHz repetition rate. The excitation laser pulse nonselectively excited antenna Chl-*a* molecules at 10 nJ/cm^2 per pulse, which hardly caused any damage to the sample. The fluorescence emitted from the sample was passed through a long-pass glass filter (R650; Toshiba, Tokyo, Japan) and focused onto the entrance slit of a monochromator (C5094; Hamamatsu Photonics, Inc., Hamamatsu, Japan). The output photons from the monochromator dispersed with respect to the wavelength were further displaced with respect to the arrival time inside the streak camera coupled to the monochromator exit. Figure 1 shows the typical wavelength−time 2-dimensional (2-D) images obtained in the photon counting mode with the present experimental setup.

For precise determination of the $-\Delta G_{CS}$ value, the ratio between the intensities of the rapidly decaying and the long-lived fluorescence is required. We measured the time-resolved fluorescence of each sample in three different time windows, i.e., 1, 10, and 100 ns. The instrumental response functions in each time window were obtained from measurements of the laser profiles in each case. The sensitivity of the experimental setup was calibrated by measuring the emission spectrum of a standard lamp.

III. Results

Decay Kinetics of the Prompt and Delayed Fluorescence in PSI. We measured the decay kinetics of the prompt and delayed fluorescence in PSI particles at 640–770 nm within 100 ns after laser excitation. Panels A and B in Figure 1 show the time−wavelength 2-D images of the fluorescence measured by a streak-camera system at 77 K in the PSI-200 particles (PSI-200) and the ether-extracted PSI-16 particles, respectively. The region with the most intense fluorescence is blue.

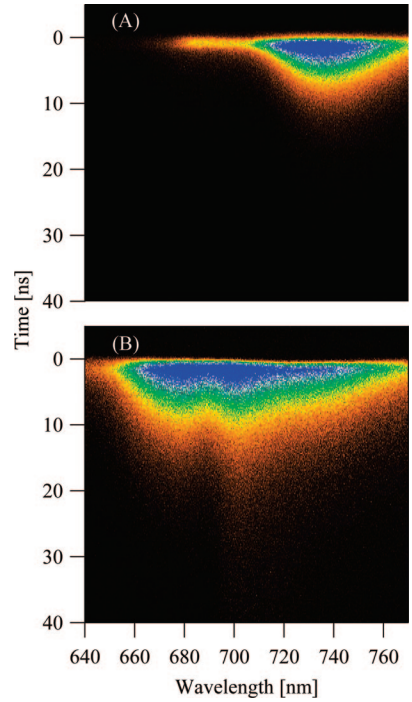

Figure 1. Wavelength−time 2-D images of the fluorescence decay in PSI-200 (A) and PSI-16 (B) at 77 K. The detected fluorescence signal increases in the order shown by the colors orange, yellow, green, and blue. See Experimental Methods for the experimental details.

The fluorescence in PSI-200 (without dithionite) showed a rapid decay at 670–700 nm, suggesting efficient energy transfer to P700 and the red Chl bands. Energy transfer to the former is trapped in the photoreaction, and that to the latter accumulates most of the excitation energy to be emitted at around 730 nm at 77 K. Almost no fluorescence was detected beyond 20 ns after excitation.

The ether-treated PSI-16 showed a somewhat different image with a slow fluorescence decay at 660–720 nm with time constants of a few nanoseconds. The slow fluorescence can be considered to be emitted from the Chls,[33,34] which are decoupled from P700 as for the energy transfer and emit fluorescence by themselves. The image, however, also shows a slowly decaying fluorescence at 700 nm that is detectable even at 40 ns after excitation, as reported previously.[33] This component gave a decay time of 35 ns, almost the same as the lifetime of the primary radical pair (RP) state $P700^+A_0^-$, which decays mainly through the charge recombination reaction and produces the triplet state ^{T}P700.[35] We, therefore, can consider this band as DF from P700* repopulated through charge recombination, as concluded in previous studies.[31–34] This interpretation can be supported by the fact that DF was suppressed by the P700 preoxidation in previous work.[33]

The time-resolved fluorescence spectra of PSI-16 at 77 and 268 K are shown as circles in Figure 2A and B, respectively. The spectra within 160 ps were calculated from the measurements with a time window of 1 ns. The one at 30–60 ns was measured with a time window of 100 ns. The solid and broken lines represent the simulated sum and component curves, respectively, calculated as described in the next section.

At 77 K, the fluorescence peak at 692 nm seen in the spectrum at 0–20 ps (Figure 2A) rapidly decayed within a few tens of picoseconds, suggesting efficient energy transfer to other Chls. Then, two other peaks appeared at 679 and 703 nm. The former, with a lifetime of 6–7 ns, can be considered to represent

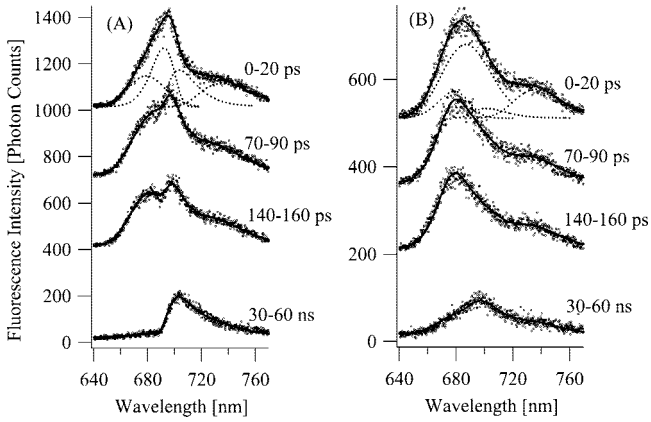

Figure 2. Time resolved-fluorescence spectrum in PSI-16 at 77 (A) and 268 K (B) and their simulated spectra. The open circles show the time-resolved fluorescence spectra of PSI-16Chl upon excitation at 405 nm. The time range after laser excitation is shown. The upper three spectra and the bottom one were obtained from the measurement of 1 and 100 ns time windows, respectively. The solid lines show the fitting curves calculated as a sum of four skewed Gaussian component functions expressed as broken lines.

fluorescence from the Chls that are decoupled from P700, as estimated previously.[31] On the other hand, the band at 703 nm, which remained even at 30–60 ns, can be considered to be DF from P700*.[33]

At 268 K, fluorescence bands overlapped due to band broadening (Figure 2B). However, the peak wavelength of the spectrum shifted from 685 to 700 nm during the decay. The 700 nm peak showed significant intensity even at 30–60 ns, suggesting it to be DF. A comparison of the fluorescence at 77 and 268 K in Figure 2 showed that the relative intensity of DF to the rapidly decaying (prompt) fluorescence does not decrease significantly even at 77 K.

Analysis of Time-Resolved Fluorescence Spectra into Spectral Component Bands. We divided a 2-D image in Figure 1 into 48 time ranges and calculated 48 time-resolved spectra as an average for each time range, as shown in Figure 2. From the measurements with the 1, 10, and 100 ns time windows, we calculated 144 time-resolved spectra altogether. The time-resolved spectra were fitted to a model curve as the sum of skewed Gaussian functions,[36,37] expressed as in eq 1

$$F(\nu) = \sum_{i=1}^{N} F_i \exp\left(-\ln 2 \cdot \left[\frac{\ln(1 + 2b_i(\nu - \nu_{\max,i})/\Delta\nu_i)}{b_i}\right]^2\right) \quad (1)$$

Here, F_i, $\nu_{\max,i}$, and $\Delta\nu_i$ are the height, peak position, and width of the ith component band, respectively. b is an asymmetry parameter that was introduced to fit the asymmetric spectral shape with the smallest number of parameters. If b is negative/positive, a model curve gives a milder slope on the lower/higher wavenumber side, and if $b = 0$, it becomes a symmetric Gaussian curve. We fitted each time-resolved spectrum by eq 1 as a function of wavenumber ν and expressed it as a function of wavelength in the figures.

We used the sum of four skewed Gaussians to fit the time-resolved spectra satisfactorily, as shown by solid lines in Figure 2. The broken lines represent each component spectrum calculated. Hereafter, we designate the four spectral components with fluorescence peaks at 679, 692, 703, and 734 nm as F679, F692, F703, and F734, respectively. In the simulation of time-resolved spectra at different delay times, we fixed parameters other than the amplitudes of four spectral components. First, we fitted the following six spectra, namely, those at 100 ps, 200 ps, 4 ns, 40 ns, and 80 ns after excitation and that integrated over the entire time range. This preliminary fitting was conducted to determine the values of $\nu_{\max,i}$, $\Delta\nu_i$, and b_i, which are assumed to be independent of time. The preliminary fitting was done under the constraint that the values of $\nu_{\max,i}$, $\Delta\nu_i$, and b_i take the same values among the above six spectra. Then, all 144 spectra were fitted under the constraint of fixed $\nu_{\max,i}$, $\Delta\nu_i$, and b_i values while varying the amplitude, F_i.

The peak wavelength, $\lambda_{\max} = 1/\nu_{\max}$, of each component varied only slightly within about ± 1 nm upon temperature change. The widths of the band, $\Delta\nu$, depended mildly on temperature except for F692, which apparently increased from 180 cm^{-1} at 77 K to 360 cm^{-1} at 268 K. We consider F692 as emitted from pigment pool containing several Chl-*a* that are tightly coupled each other. The increase in the width of F692 upon temperature increase might be due to the equilibrium of the excited states over more pigments in the pool at higher temperatures. The other fluorescence components seem to be emitted from pigment pools that consist of a lower number of Chl-*a* molecules in almost similar environments. The temperature-dependent changes in the bandwidth of F692 (a major component of prompt fluorescence) affected the quality of curve fitting. However, it did not significantly affect the quantitative estimation of the relative amplitudes of prompt and delayed fluorescence components because of the very fast decay time of F692.

Figure 3 shows a log–log plot of the time-dependent changes in the spectral areas of F679 (blue), F692 (green), F703 (orange), and F734 (red) at 268 (A), 180 (B), and 77 K (C). Peak height in the time course of F703 was normalized to unity. Figure 3(inset) shows the instrumental response function in each time window. The solid lines in the inset show the fitting curves to Gaussian functions that have full-widths at half-maximum of 77 ps, 220 ps, and 1.8 ns for 1, 10, and 100 ns time windows, respectively. In the figure the time of the excitation is set at the origin of time in the horizontal axis. The time course obtained from measurements in the 1, 10, and 100 ns time windows are shown as open circles, open triangles, and crosses, respectively, normalized by the F703 peak. The solid lines represent the fitting curves obtained as the sum of the exponential decay functions, which were convolved with the Gaussian fitting curves of the instrumental response functions shown in Figure 3(inset).

F703 was fitted with the one rising and four decaying exponential components containing the long-lived DF component, which was estimated to have a 33 ns decay time constant at 77 K with an amplitude of 0.66% with respect to the sum of the amplitudes of the four decaying components. F734 also contained the 33 ns DF component. The DF component could be either the shoulder band of F703 or the emission from the red antenna Chls, which is expected to remain at about 0.1 molecules per P700.[5,34] In addition to these DF components, decay components with 2–6 ns time constants are also required to fit the time courses of F703 and F734 satisfactorily, as shown in Figure 3 and listed in detail in Table 1. Some of these components might represent the fluorescence from the Chls decoupled for energy transfer to P700.

A rapid 75 ps decay component contributed mainly to the time course of F692 at 77 K, suggesting excitation energy transfer from F692 to F703. The rise components were detected in the time courses of both F703 and F679. We can interpret the rapid decay in F692 to be due to the energy transfer to F703 but not to F679 because the uphill energy transfer from F692

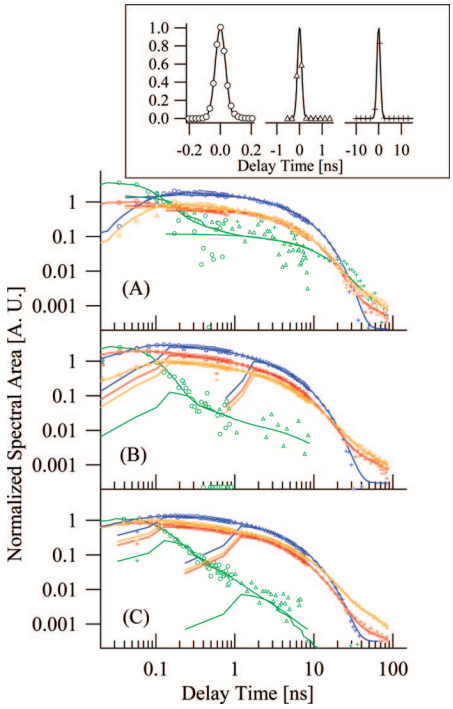

Figure 3. Time course of the area of each fluorescence band at different temperatures. The spectral area of F679 (blue), F692 (green), F703 (orange), and F734 (red) at 268 (A), 180 (B), and 77 (C) are plotted against the delay time from the laser excitation. The open circles, open triangles, and crosses are the data points obtained from measurements of the time windows of 1, 10, and 100 ns, respectively. All intensities are normalized by adjusting the peak intensity of F703 to be unity. The solid lines are the fitting curves calculated as the sum of five exponential functions convoluted with the instrumental response functions. The inset shows the instrumental response function in each time window. Solid lines in the inset are the fitting curves to the Gaussian function.

to F679 can be assumed to be negligible. The time constant of the rise of F703 was not always in good agreement with that of the rapid decay of F692 probably due to the uncertainty in the determination of the rise times of the overlapping components. F679 was fitted by one 53 ps rise and three (0.34, 2.0, and 4.9 ns) decaying components (not shown in detail in Table 1). Neither the DF component nor the rapidly decaying components faster than 100 ps were necessary to fit the time course of F679 simulated at all temperatures. The result supports the interpretation that F679 is emitted from the decoupled Chls.

We summarized the results of the kinetic fitting of F703, F734, and F692 in Table 1. The values of the amplitude in Table 1 are normalized to give the sum of four decaying components of F703 to unity. Figure 3 and Table 1 clearly indicate that the time constant and relative amplitude of DF components depend on the temperature only weakly.

Estimation of ΔG_{CS} for Production of DF. Figure 4 shows a model formulated to account for the PSI DF. The model involves two fluorescent compartments, ant692, the antenna Chls that emit F692, and P*, the excited state of the primary donor. P* is assumed to emit F703. F734 was assumed to be the mixture of fluorescence at the red tail of F679, F692, and F703. The model involves two nonfluorescent compartments, the primary radical pair (RP) and the triplet state of the primary donor (^{T}P). k_{LH}, k_{+}, k_{-}, and k_{CR} in Figure 4 are the rates of the energy transfer from ant692 to P*, the primary charge separation, the uphill charge recombination to P*, and the decay of RP state, respectively.

F679 can be assumed to be emitted from Chl molecules that are inactive as antennae and decoupled from P for the energy transfer. We observed no rapid decay with a time constant shorter than 100 ps in the F703 decay and detected the rapid decay of F692 with a time constant of a few tens of picoseconds. Figure 3 clearly shows that only F692 shows such rapid decay, suggesting that the major path for excitation in PSI-16 is from ant692 to P*. The reason for the F703 decay with a time constant of a few nanoseconds is not clear yet.

We formulated the relation between the kinetic parameters obtained in the previous section and the standard free-energy difference ΔG_{CS} in the RC containing active antenna Chls. The population of the excited state in each compartment in Figure 4 obeys the rate equations

$$\begin{aligned}\frac{d[\text{ant692}]}{dt} &= -k_{LH}[\text{ant692}] \\ \frac{d[P^*]}{dt} &= k_{LH}[\text{ant692}] - k_{+}[P^*] + k_{-}[RP] \\ \frac{d[RP]}{dt} &= k_{+}[P^*] - (k_{-} + k_{CR})[RP]\end{aligned} \tag{2}$$

Here, the relaxation processes from the excited state by the fluorescence emission and the radiationless heat process were neglected because of their slower rates than k_{LH} and k_{+}. By assuming the equilibration between P* and RP and the initial conditions of [ant692]($t = 0$) = 1 and [P*]($t = 0$) = 0, we obtain the following relations

$$\begin{aligned}[\text{ant692}] &= \exp(-k_{LH}t) \\ [P^*] &= \frac{k_{-}}{k_{+}+k_{-}}(1-\exp(-k_{LH}t))\exp\left(-\frac{k_{+}}{k_{+}+k_{-}}k_{CR}t\right)\end{aligned} \tag{3}$$

We consider here the spectral areas of the fluorescence from ant692 and P* are proportional to the populations of excited states on [ant692] and [P*], respectively. We interpret that the fastest decay component in F692 is due to the light-harvesting process (with a rate constant of k_{LH}) and that the slowest decay components of F703 and 734 are emitted as DF. Finally, we obtain the relation

$$\exp\left(\frac{\Delta G_{CS}}{k_B T}\right) = \frac{k_{-}}{k_{+}} = \frac{A_{\text{ant692}}}{A_{\text{ant692}} - A_{DF}} \tag{4}$$

Here A_{ant692} is the pre-exponential factor of the fastest fluorescence decay component in the time course of F692, while A_{DF} is the sum of the pre-exponential factors of the slowest decay components of F703 and F734. It is noteworthy in eq 4 that the ΔG_{CS} value can be calculated using the ratio between the pre-exponential factors of the fastest decay in F692 and the slowest decay in F703, which can be readily available from Figure 3.

In the intact PSI particle, we should take into account the contribution of the red antenna Chls that might accept energy from P* and apparently decrease the ΔG_{CS} value by stabilizing the excited state in competition with the primary charge separation.[21] In the ether-extracted PS I, most of the red Chls are removed so that the estimated ΔG_{CS} value is highly reliable together with the adaptation of the deconvolution analysis which distinguished the fluorescence components of the active antenna and P*.

Kumazaki et al.[5] reported the decay-associated difference absorption spectrum with a negative peak at 680 nm and a positive peak at 696 nm with a time constant of 10.1 ps in PSI-16 particles upon excitation at 662 nm. This 10 ps process seems to correspond to the energy-transfer process from F692 to the RC observed in the present study. The slower time constants

TABLE 1: Kinetic Parameters for the Fluorescence Components

T [K]			A_1 [ns]	τ_1	A_2 [ns]	τ_2	A_3 [ns]	τ_3	A_4 [ns]	τ_4 10^{-2}	A_5 [ns]
77	F703	−1.1	0.016	0.43	0.24	0.37	2.3	0.19	6.0	0.66	33
	F734	0.20	0.056	0.23	0.31	0.34	2.5	0.12	6.0	0.11	33
	F692	1.7	0.075	0.085	0.43						
148	F703	−0.10	0.071	0.50	0.37	0.37	2.7	0.13	6.0	0.73	35
	F734	−2.6	0.011	0.34	0.26	0.38	2.2	0.17	5.3	0.18	35
	F692	3.0	0.050	0.043	0.51						
180	F703	−1.5	0.035	0.35	0.29	0.50	2.3	0.15	6.6	0.46	40
	F734	0.57	0.12	0.51	0.68	0.60	2.5	0.24	5.4	0.32	40
	F692	4.9	0.050	0.058	0.39						
210	F703	−1.2	0.075	0.52	0.19	0.32	1.9	0.16	5.1	0.32	30
	F734	0.34	0.30	0.15	1.2	0.24	2.5	0.14	5.1	0.12	30
	F692	2.8	0.068	0.13	0.95						
240	F703	−1.4	0.070	0.61	0.13	0.29	1.9	0.10	5.7	0.23	35
	F734	0.83	10.026	0.31	0.24	0.31	2.3	0.098	5.5	0.41	35
	F692	4.8	0.041	0.28	0.30						
268	F703	−1.7	0.046	0.33	0.50	0.35	3.0	0.32	5.8	0.73	37
	F734	0.55	0.036	0.41	0.11	0.38	3.6	0.26	6.0	0.28	37
	F692	7.1	0.054	0.36	0.30						

of 54/75 ps estimated at 268/77 K in the present study (Table 1) seem to reflect the slower time resolution and the significantly nonselective excitation in the present experimental system. Although the origin of F692 is not clear, it cannot be emitted from A_0 or accessory Chls that are tightly coupled to the RC.

Figure 5A shows the temperature dependences of A_{ant692} (the pre-exponential factor of the fastest decay component of F692) and A_{DF} (the sum of the pre-exponential factors of DF as the slowest decay components in F703 and F734). Both amplitudes showed weak temperature dependences. We calculated the $-\Delta G_{CS}$ values according to eq 4 and plotted them versus the temperature in Figure 5B. The $-\Delta G_{CS}$ value of spinach PSI-16 at room temperature can be estimated to be ∼150 meV, which is consistent with the previous estimation by Iwaki et al.[10] and somewhat smaller than the value of 250 meV calculated for the PSI of the *Synechocystis* PCC6803 mutant in the presence of dithionite to reduce A_1 at 2–25 °C.[21] Here, $-\Delta G_{CS}$ values were estimated from the A_{DF} values with both F703 and F734 contributions by assuming F734 to be the long-wavelength shoulder band of F703. Contrary to the above assumption, if F734 is emitted from the remaining red antenna Chls, the relative contribution from F734 to DF should drastically increase upon cooling because of the enhanced population in the excited red Chls at low temperatures. This is not the case as shown in Table 1, and then we neglected the possibility that F734 is emitted from the remaining red antenna Chls.

DF in PSI-200 in the Presence of Dithionite. We also measured DF in the untreated PSI particles. We irradiated the PSI particle in the presence of sodium dithionite at pH 10.5 and designated the sample as dtPSI-200. This procedure is known to photoaccumulate the iron−sulfur centers F_A^-, F_B^-, and F_X^- and increase the reduced phylloquinones (A_1), at least partially, under illumination as reported by Kleinherenbrink et al.[21] Electron transfer from A_0^- to A_1 is expected to be blocked and give the higher DF due to the enhanced charge recombination reaction between $P700^+$ and A_0^-. The time-resolved fluorescence spectra in dtPSI-200 at 77 and 297 K are shown in panels A and B in Figure 6. The spectra at 30–60 ns at 297 K clearly indicated the DF component with a spectral feature similar to that reported by Kleinherenbrink et al.[21] in the dithionite-reduced PSII-less *Synechocystis* mutant PSI. The DF component, thus, can be assumed to be emitted from the charge-recombination reaction in the PSI RC. The slow decay

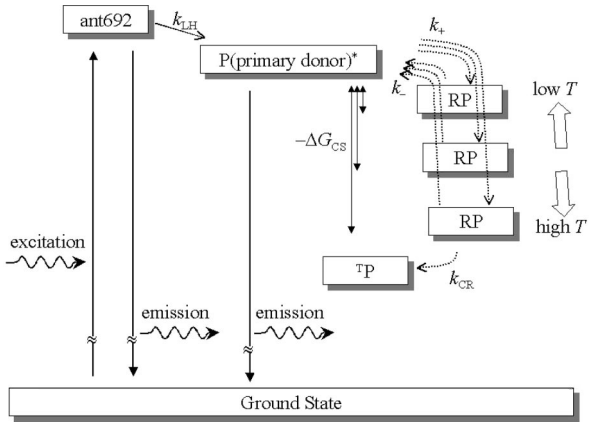

Figure 4. Scheme for energy transfer and charge separation in PSI-16. The boxes correspond to the kinetic compartments. The vertical axis indicates the free energy change. The energy transfer from ant692 to the primary donor (P) is expressed with an inclined arrow and the electron-transfer processes with arrows with dashed lines. Radical pair (RP) states with various $-\Delta G_{CS}$ values are depicted, reflecting the temperature-dependent $-\Delta G_{CS}$ values, as indicated by the present experiment.

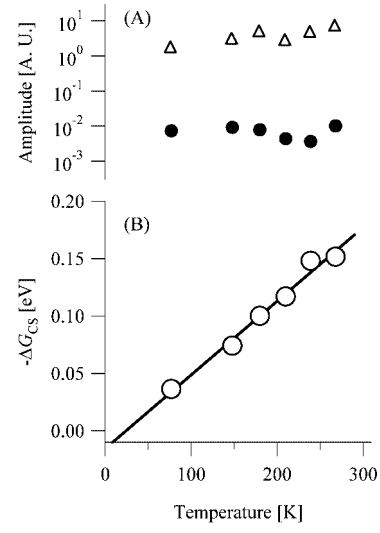

Figure 5. (A) Temperature dependence of the amplitudes of prompt fluorescence (open triangles) and DF (closed circles). See text for assignment of prompt and delayed fluorescence. (B) Temperature dependence of the estimated $-\Delta G_{CS}$ value. The solid line shows the fitting to a linear line.

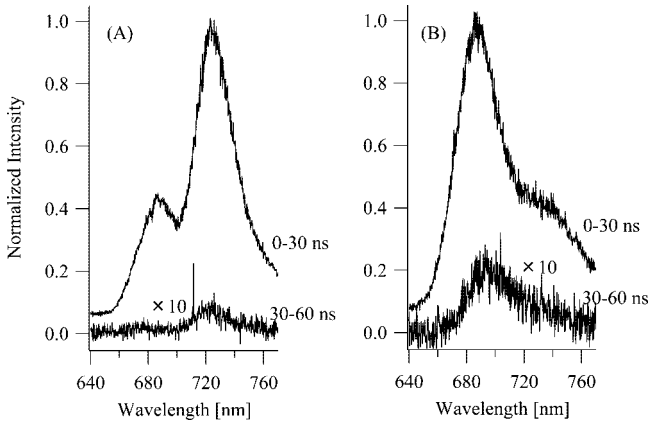

Figure 6. Time-resolved fluorescence spectra at 297 and 77 K in dtPSI-200. The solid lines show the temporal change in the fluorescence spectra at 77 (A) and 297 K (B) of dtPSI-200 in which the acceptor quinone is reduced by addition of 50 mM sodium dithionite. The excitation wavelength was at 405 nm. The numbers on the right of the spectra indicate the time ranges after laser excitation over which the spectra are accumulated.

component in the fluorescence kinetics at 700−730 nm was well fitted to an exponential decay with a time constant of 22 ns at 297 K and 37 ns at 77 K (data not shown).

At 77 K, the spectrum of the prompt fluorescence measured within 30 ns showed a peak at 730 nm, indicating its emission mainly from the excited long-wavelength antenna Chls, as is well known.[1,32,38] It is noteworthy that the DF peak at 30–60 ns was also observed at 730 nm, indicating its emission from the same bulk antenna red Chls. The relative intensity of DF somewhat decreased at 77 K but was still high enough to be detected, suggesting a very small $-\Delta G_{CS}$ value at 77 K for its production in this case. The weak temperature dependence of the relative DF yield at 276–77 K in dtPSI-200 was similar to that detected in the PSI-16 particles. The equilibrium between the excited red Chls and P* makes estimation of the $-\Delta G_{CS}$ value rather complex as suggested by Kleinherenbrink et al.[21] At low temperatures, the uphill energy transfer from the red Chls to P* can be assumed to be almost completely inhibited. Then the equilibrium between the two pigment pools does not hold. This situation causes uncertainty in the quantitative estimation of the $-\Delta G_{CS}$ value. In addition, the amount of RC with the photoaccumulated A_1^- is not clear as discussed above. Thus, we did not calculate the $-\Delta G_{CS}$ value for dtPSI-200. However, the result clearly indicates that the mechanisms of DF production are similar in the two preparations, although PSI-200 emits prompt fluorescence and DF mainly as F730 from the long-wavelength antenna Chls.

The assignment of the primary electron donor in PSI to be either P700 or the accessory Chl-*a* is still under debate;[6,7] however, the conclusion of the lower $-\Delta G_{CS}$ value at a lower temperature in PSI still stands.

IV. Discussion

The present study in the spinach PSI-16, which lacks the secondary acceptor phylloquinone and 90% of antenna Chls, revealed that the $-\Delta G_{CS}$ value in the primary charge separation decreases on cooling. The temperature dependence was also confirmed in spinach dtPSI-200, which has phylloquinone in the reduced state and all the antenna Chls. The results in PSI-16 and dtPSI-200 are very similar to the features of the $-\Delta G_{CS}$ values estimated by DF in PSII[19,20] and the purple bacterial RCs.[18]

We should first consider the possibility that PSI-16 has defects in the multiple electron carriers in addition to the known loss of phylloquinone. We confirmed that if P700 was inactivated (if insensitive to redox reagents) during the harsh ether treatment in some cases, no DF was emitted. However, even a 10% contamination of such damaged PSI will modify the $-\Delta G_{CS}$ value less than 1% due to the dependence of the ΔG_{CS} value on the logarithm of the relative amplitude of DF, as shown in eq 4.

The temperature dependence of the free-energy difference $-\Delta G_{CS}$ of the charge recombination in Figure 5B gives the value of the enthalpy change, $-\Delta H_{CS}$, and the entropy change, ΔS_{CS}, to be −16 meV and +0.64 meV/K, respectively. These values suggest the 90% contribution of the entropy difference to the total $-\Delta G_{CS}$ at room temperature. If we assume $-\Delta H_{CS}$ and ΔS_{CS} to be temperature independent, we should expect a negligible enthalpy contribution at room temperature.

As discussed by Edens et al.,[14] the movement of ions and water molecules at the RC surface may induce a large entropy change after the ET reaction. We can expect suppression of these molecular movements and a decrease in ΔS_{CS} upon cooling below 0 °C. This should be reflected in the reduction in the slope of the $-\Delta G_{CS}-T$ plot upon lowering temperature. However, it was not the case in Figure 5B. Therefore, we assume the primary charge separation to be either (1) entropy driven with the *T*-independent ΔS_{CS} value over a wide temperature range or (2) enthalpy driven with *T*-dependent ΔH_{CS}. If 1 is the case, we have no idea at present how a large *T*-independent entropy change is realized in the primary charge separation of RC. Hypothesis 2 seems to be consistent with the idea[20,26,39] that the temperature-dependent $-\Delta H_{CS}$ is related to suppression of the protein relaxation that lowers the free-energy change for stabilization of the RP state at lower temperature. It has been assumed that the RP relaxes to the state with a large $-\Delta H_{CS}$ value at room temperature but is trapped in an unrelaxed substrate with a smaller $-\Delta H_{CS}$ value at lower temperature. Xu and Gunner[26] revealed that the $-\Delta H_{CS}$ of the charge-recombination reaction of the $P^+Q_A^-$ state through the P^+H^- state in the bacterial RC was drastically decreased below a transition temperature of around 200 K, presumably through suppression of protein relaxation.

The different sensitivities of the thermodynamic properties of the RC to the time scale of the measurements suggest the effects of protein relaxation on the ET reaction. Edens et al.[14] obtained a smaller $-\Delta H_{CS}$ value in the bacterial RC by a photoacoustic measurement than by a DF measurement. The photoacoustic measurement is more sensitive to submicrosecond events, while the DF measurement is more sensitive to the millisecond events in the bacterial RC. They interpreted the discrepancy of the $-\Delta H_{CS}$ values between the two methods to be related to protein relaxation, which continues longer than the time scale of the photoacoustic measurement. Protein relaxation is known to be distributed over a wide time range from picoseconds to milliseconds.[40,41]

Holzwarth et al. recently proposed that three RP states in the initial ET reaction in PSI are required to interpret the ultrafast transient absorption changes[6,7] and fluorescence kinetics.[42] They proposed a model of ET in the PSI RC by postulating three RP states, $A_{acc}^+A_0^-$, $P700^+A_0^-$, and $P700^+A_1^-$. Here, A_{acc}^+ denotes the cation radical of the accessory Chl-*a*. The model, which assumes the primary electron donor to be A_{acc}, thoroughly explained the experimental results with the wild-type and mutant PSI. On the basis of this type of model, the primary and secondary RP states in PSI-16 can be assigned to $A_{acc}^+A_0^-$ and

$P700^+A_0^-$, respectively. The temperature-dependent $-\Delta G_{CS}$ value observed in the present study can, then, be interpreted as coming from inhibition of ET from the primary to secondary RP state upon cooling. In this interpretation it is assumed that the ET to the secondary RP state is active only at high temperatures. However, $P700^+A_0^-$, which is the secondary RP state in this model, seems to be populated even at 77 K. The DF measurement will then give the $-\Delta G_{CS}$ value of the secondary RP state even at low temperature. This model, thus, cannot easily interpret the temperature-dependent $-\Delta G_{CS}$ value observed in this study.

Holzwarth et al.[7,42] also proposed an ET scheme involving protein relaxation. In their scheme A_{acc} was not assumed to be an electron carrier and multiple RP states with the same electronic configuration in different protein relaxation states were considered. They, however, excluded this scheme because the conformation change after relaxation does not interpret the spectral difference between the two RP states that they had observed. We, however, believe that the temperature-dependent $-\Delta G_{CS}$ value detected in this study can be explained by this scheme. The high $-\Delta G_{CS}$ values obtained at higher temperatures may reflect the fully relaxed protein conformation, while those at lower temperatures with smaller values may reflect the unrelaxed semistable states due to the restricted protein relaxation during the measurement of DF (i.e., within a few tens of nanoseconds after laser excitation).

The idea that both the A and B branches of the ET pathways in the PSI RC are active to different extents has received more support recently.[8,43,44] If the $-\Delta G_{CS}$ value is different in the RP states formed in the A and B branches and the distribution of the ET between the two branches is temperature dependent, the apparent $-\Delta G_{CS}$ value will also depend on the temperature. This interpretation will be applicable only to PSI because the electron-transfer reactions occur along only one branch in PSII[19,20] and purple bacterial[18] RCs. The temperature-dependent $-\Delta G_{CS}$ values reported in these RCs are, however, very similar to that observed in PSI in this study.

The $-\Delta G_{CS}$ value obtained was 160/36 meV at 268/77 K in PSI-16, and it had a slightly larger value of 280/81 meV at 297/77 K in dtPSI-200. It is clear that both samples showed temperature-dependent $-\Delta G_{CS}$ values but with different values. Although the reason for the difference is not clear yet, it might partially come from the different levels of the DF-emitting Chls. It is also possible that extraction of phylloquinone had a somewhat additional effect compared to the simple chemical reduction of phylloquinone on the energy level of the RP state.

V. Concluding Remarks

The present study clarified that PSI RC shows DF even at 77 K. The temperature-independent yield of DF in the ether-extracted PSI indicates that the apparent $-\Delta G_{CS}$ value decreases with the decrease of the temperature. A similar temperature dependence was also reported for the DF in PSII[19,20] and in bacterial RCs.[18] The decreases in the apparent $-\Delta G_{CS}$ values at low temperature are thus shown to be common phenomena among types I and II RCs. One explanation for this is that the larger protein relaxation stabilizes the RP state more at higher temperatures and that the RP is trapped at higher unrelaxed energy levels at lower temperatures, giving lower $-\Delta G_{CS}$ values, as proposed for type II RCs.[20,26,39] However, it is not fully clear at present how the protein relaxation modifies the free energy of RP. The mechanism implies that the secondary ET reaction that occurs within a few picoseconds takes place from the RP in the unrelaxed protein conformation. This may be important to re-evaluate the mechanisms of fast ET reactions inside the RCs because the standard Marcus theory assumes a Franck–Condon-type relaxation of molecular states in the reactant state before the ET.[27]

Acknowledgment. The work was supported in part by Grants-in-Aid for Scientific Research (No. 17750010), the 21st COE program for "The Origin of the Universe and Matter" from the Japanese Ministry of Education, Science, Sports, and Culture (MEXT), and the Japan Society for the Promotion of Science.

Supporting Information Available: Time course of the florescence intensity at 730 nm of dtPSI-200 under irradiation of blue light and in a reaction medium containing 50 mM sodium dithionite at pH 10.5, suggesting photoaccumulation, at least partially, of the reduced A_1. This material is available free of charge via the Internet at http://pubs.acs.org.

References and Notes

(1) Golbeck, J. H. In *The Molecular Biology of Cyanobacteria*; Bryant, D. A., Ed.; Kluwer Academic Publishers: Dordrecht, 1994; p 319.
(2) Diner, B. A.; Babcock, G. T. In *Oxygenic Photosynthesis: The Light Reactions*; Ort, D. R., Yocum, C. F., Eds.; Kluwer Academic Publishers: Dordrecht, 1996; p 13.
(3) Brettel, K. *Biochim. Biophys. Acta* **1997**, *1318*, 322.
(4) Kumazaki, S.; Ikegami, I.; Furusawa, H.; Yasuda, S.; Yoshihara, K. *J. Phys. Chem. B* **2001**, *105*, 1093.
(5) Kumazaki, S.; Ikegami, I.; Furusawa, H.; Yoshihara, K. *J. Phys. Chem. B* **2003**, *107*, 3228.
(6) Müller, M. G.; Niklas, J.; Lubitz, W.; Holzwarth, A. R. *Biophys. J.* **2003**, *85*, 3899.
(7) Holzwarth, A. R.; Müller, M. G.; Niklas, J.; Lubitz, W. *Biophys. J.* **2006**, *90*, 552.
(8) Santabarbara, S.; Heathcote, P.; Evans, M. C. W. *Biochim. Biophys. Acta* **2005**, *1708*, 283.
(9) Gunner, M. R.; Dutton, P. L. *J. Chem. Am. Soc.* **1989**, *111*, 3400.
(10) Iwaki, M.; Kumazaki, S.; Yoshihara, K.; Erabi, T.; Itoh, S. *J. Phys. Chem. B* **1996**, *100*, 10802.
(11) Jordan, P.; Fromme, P.; Witt, H. T.; Klukas, O.; Saenger, W.; Krauss, N. *Nature* **2001**, *411*, 909.
(12) Ben-Shem, A.; Frolow, F.; Nelson, N. *Nature* **2003**, *426*, 630.
(13) Arata, H.; Parson, W. W. *Biochim. Biophys. Acta* **1981**, *636*, 70.
(14) Edens, G. J.; Gunner, M. R.; Xu, Q.; Mauzerall, D. *J. Am. Chem. Soc.* **2000**, *122*, 1479.
(15) Hou, J. M.; Boichenko, V. A.; Diner, B. A.; Mauzerall, D. *Biochemistry* **2001**, *40*, 7117.
(16) Hou, H. J. M.; Mauzerall, D. *J. Am. Chem. Soc.* **2006**, *128*, 1580.
(17) Arata, H.; Parson, W. W. *Biochim. Biophys. Acta* **1981**, *638*, 201.
(18) Woodbury, N. W.; Parson, W. W.; Gunner, M. R.; Prince, R. C.; Dutton, P. L. *Biochim. Biophys. Acta* **1986**, *851*, 6.
(19) Booth, P. J.; Crystall, B.; Giorgi, L. B.; Barber, J.; Klug, D.; Porter, G. *Biochim. Biophys. Acta* **1990**, *1016*, 141.
(20) Booth, P. J.; Crystall, B.; Ahmad, I.; Barber, J.; Porter, G.; Klug, D. *Biochemistry* **1991**, *30*, 7573.
(21) Kleinherenbrink, F. A.; Hastings, G.; Wittmerhaus, B. P.; Blankenship, R. E. *Biochemistry* **1994**, *33*, 3096.
(22) Klevanik, A. *Biochim. Biophys. Acta* **1996**, *1275*, 237.
(23) Turzó, K.; Laczkó, G.; Filus, Z.; Maróti, P. *Biophys. J.* **2000**, *79*, 14.
(24) Goldstein, R. A.; Takiff, L.; Boxer, S. G. *Biochim. Biophys. Acta* **1988**, *934*, 253.
(25) Polm, M.; Brettel, K. *Biophys. J.* **1998**, *74*, 3173.
(26) Xu, Q.; Gunner, M. R. *Biochemistry* **2001**, *40*, 3232.
(27) Marcus, R. A.; Sutin, N. *Biochim. Biophys. Acta* **1985**, *811*, 265.
(28) Ikegami, I.; Katoh, S. *Biochim. Biophys. Acta* **1975**, *376*, 588.
(29) Ikegami, I.; Ke, B. *Biochim. Biophys. Acta* **1984**, *764*, 70.
(30) Kumazaki, S.; Ikegami, I.; Yoshihara, K. *J. Phys. Chem.* **1997**, *101*, 597.
(31) Ikegami, I.; Iwaki, M.; Itoh, S. *Plant Cell Physiol.* **2000**, *35*, 983.
(32) Itoh, S.; Iwaki, M.; Ikegami, I. *Biochim. Biophys. Acta* **2001**, *1507*, 115.
(33) Itoh, S.; Iwaki, M. *Biochim. Biophys. Acta* **1988**, *934*, 32.
(34) Iwaki, M.; Mimuro, M.; Itoh, S. *Biochim. Biophys. Acta* **1992**, *1100*, 278.
(35) Ikegami, I.; Sétif, P.; Mathis, P. *Biochim. Biophys. Acta* **1987**, *894*, 414.

(36) Sevilla, J. M.; Dominguez, M.; Garcia-Blanco, F.; Blazquez, M. *Comput. Chem.* **1989**, *13*, 197.

(37) Hoff, W. D.; Van Stokkum, I. H. M.; van Ramesdonk, H. J.; van Brederode, M. E.; Brouwer, A. M.; Fitch, J. C.; Meyer, T. E.; van Grondelle, R.; Hellingwerf, K. J. *Biophys. J.* **1994**, *67*, 1691.

(38) Itoh, S.; Sugiura, K. In *Chlorophyll a Fluorescence: A Signature of Photosynthesis*; Papageorgiou, G. C., Govindjee, Eds.; Springer: Dordrecht, 2004; p 231.

(39) McMahon, B. H.; Müller, J. D.; Wraight, C. A.; Nienhaus, G. U. *Biophys. J.* **1998**, *74*, 2567.

(40) Shibata, Y.; Kurita, A.; Kushida, T. *Biochemistry* **1999**, *38*, 1789.

(41) Green, J. L.; Fan, J.; Angell, C. A. *J. Phys. Chem.* **1994**, *98*, 13780.

(42) Holzwarth, A. R.; Müller, M. G.; Niklas, J.; Lubitz, W. *J. Phys. Chem. B* **2005**, *109*, 5903.

(43) Agalarov, R.; Brettel, K. *Biochim. Biophys. Acta* **2003**, *1604*, 7.

(44) Guergova-Kuras, M.; Boudreaux, B.; Joliot, A.; Joliot, P.; Redding, K. *Proc. Natl. Acad. Sci. U. S. A.* **2001**, *98*, 4437.

JP710551E